Electronics Letters

LETTER OPEN ACCESS

Beyond Fixed Waveforms: Adaptive Angle-Dependent Design for Next-Generation 3D Radar Systems

Amgad A. Salama[1] | Ahmed Gamal Abdellatif Ibrhaim[2] | Syed Tariq Shah[3] | Ahmad Almogren[4] | Mahmoud A. Shawky[1,3]

[1]Egyptian Technical Research and Development Centre, Cairo, Egypt | [2]Faculty of Computers & Information Systems, Egyptian Chinese University, Cairo, Egypt | [3]School of Computer Science & Electronic Engineering, University of Essex, Colchester, UK | [4]Chair of Cyber Security, Department of Computer Science, College of Computer & Information Sciences, King Saud University, Riyadh, Saudi Arabia

Correspondence: Syed Tariq Shah (syed.shah@essex.ac.uk) | Ahmad Almogren (Ahalmogren@ksu.edu.sa)

Received: 4 February 2026 | **Revised:** 29 April 2026 | **Accepted:** 4 May 2026

ABSTRACT

Traditional radar systems use fixed waveform parameters, degrading performance for targets at extreme angular positions. This study analyses angle-dependent waveform design for 3D radar, dynamically adjusting parameters with target position. Modulation functions for bandwidth and pulse duration are introduced, and their effects on key performance metrics are evaluated. Mathematical analysis and simulations show marked gains in range resolution and estimation accuracy, with up to 75% improvement for high-elevation targets. Results validate the theoretical benefits of this adaptive approach over fixed-parameter waveforms, offering a practical enhancement for modern phased array radars engaging targets across diverse angular positions.

1 | Introduction

Modern radar systems face increasing demands for wide-field performance in 3D surveillance and tracking. Conventional designs often employ fixed waveform parameters, such as bandwidth (BW) and pulse duration, irrespective of target angle relative to boresight; while simplifying implementation, this often degrades performance at extreme angles [1]. Although recent advances in cognitive and adaptive radar demonstrate the value of dynamically tuning parameters to environmental conditions [2, 3], most efforts focus on transmit waveform adaptation for detection under interference [4], EMI mitigation [5] or target classification [6]. Exploiting waveform adaptation specifically regarding target angular position remains largely unexplored. Note that certain adaptation objectives are inherently contradictory: extending pulse duration for SNR and Doppler discrimination increases susceptibility to repeater jamming, while wide-bandwidth operation for high-elevation coverage complicates partial-band interference mitigation. Such trade-offs are acknowledged herein as open challenges for future robust design. Because radar-target geometry introduces angle-dependent effects, such as off-boresight range resolution degradation and varying SNR due to antenna patterns [7], wide-coverage phased arrays are affected. Leveraging adaptive waveform design [8, 9], this work investigates tuning parameters based on estimated target angles.

Recent advances in phased array radar enable feasible angle-dependent optimization. Digital beamforming arrays can transmit distinct waveforms in multiple directions simultaneously [10], facilitating such designs without major hardware changes, while real-time processing supports rapid computation of optimal parameters [11, 12]. Using the Cramér–Rao bound (CRB) framework, this work quantitatively evaluates parameter-estimation accuracy gains of the angle-dependent approach over fixed-parameter waveforms. The main contributions include: (i) an angle-dependent waveform framework for 3D radar using modulation functions to adapt bandwidth and pulse duration to target angular position; (ii) a CRB analysis quantifying gains in range resolution, SNR and estimation accuracy; and (iii) extensive simulations demonstrating up to 75% improvement in

range estimation for high-elevation targets without significant hardware modifications.

2 | Radar Performance Metrics

This section details the mathematical framework and the key metrics affected by waveform parameters.

2.1 | Mathematical Framework

The framework is established by defining angle-dependent waveform functions and their modulation forms.

2.1.1 | Angle-Dependent Waveform Functions

The angle-dependent functions for the key waveform parameters are defined as:

$$B(\theta,\phi) = B_0 f_B(\theta,\phi), \quad T(\theta,\phi) = T_0 f_T(\theta,\phi) \tag{1}$$

where B_0 and T_0 are default parameters, and f_B and f_T are modulation functions dependent on the elevation angle θ and azimuth angle ϕ.

2.1.2 | Specific Modulation Functions

For practical implementation, we propose the following modulation functions.

$$f_B(\theta,\phi) = \frac{1}{\cos\theta}, \quad f_T(\theta,\phi) = 1 + \sin^2\theta \tag{2}$$

where $f_T(\theta,\phi)$ extends pulse duration at angles with lower expected SNR while satisfying operational constraints. The modulation functions in Equation (2) apply adaptation in the elevation dimension only. This choice is motivated by the assumed antenna layout: a planar phased array with a wide horizontal aperture and a narrow vertical aperture, typical of ground-based 3D surveillance radars. The resulting narrow azimuth beamwidth limits the useful dwell time at each azimuth position, making azimuth-dependent pulse extension impractical without causing beam overlap. In elevation, the wider beamwidth and cosecant-squared scan pattern create a strong SNR gradient that $f_T(\theta,\phi)$ is designed to compensate. At large azimuth scan angles, the projected aperture provides a partial $\cos\phi$ bandwidth reduction that limits azimuth range-resolution degradation without additional time extension.

2.2 | Radar Performance Metrics

The key performance metrics affected by waveform parameters include:

2.2.1 | Range/Angular Resolution

The range/angular resolutions are given by

$$\Delta R = \frac{c}{2B}, \quad \Delta\theta \approx \frac{\lambda}{D\cos\theta}, \tag{3}$$

where B is the bandwidth, λ is the wavelength, c is the light speed, D is the aperture width and θ is the elevation angle.

2.2.2 | Signal-to-Noise Ratio (SNR)

From the standard radar range equation [7, 13], the matched-filter output SNR for a pulsed waveform of duration T and bandwidth B is:

$$\mathrm{SNR} \propto \frac{P_t G^2 \lambda^2 \sigma}{(4\pi)^3 R^4 k T_0 B F_n} \cdot T \tag{4}$$

where P_t is transmit power, G is antenna gain, σ is target radar cross-section, R is range, k is Boltzmann's constant, T_0 is reference temperature, F_n is receiver noise figure and T is pulse duration. The product $T \cdot B$ is the waveform's time-bandwidth product; linearly increasing T at fixed B improves SNR, a principle exploited by $f_T(\theta,\phi)$.

3 | Theoretical Analysis of Improvement

3.1 | Angular-Dependent Range Resolution

For targets at non-zero elevation angles, the effective range resolution is:

$$\Delta R(\theta,\phi) = \frac{c}{2B(\theta,\phi)} = \frac{c\cos\theta}{2B_0} \tag{5}$$

When projected along the line-of-sight (LoS), the effective range resolution becomes:

$$\Delta R_{\text{effective}} = \Delta R(\theta,\phi)\cdot\cos\theta = \frac{c}{2B_0} \tag{6}$$

This compensates for the geometric projection that would otherwise degrade resolution at extreme angles.

3.2 | Pulse Duration Optimization

By setting $f_T(\theta,\phi) > 1$ for angles with lower expected SNR, this achieves an SNR improvement of:

$$\Delta\mathrm{SNR}(\theta,\phi) = 10\log_{10}(f_T(\theta,\phi))\ \mathrm{dB} \tag{7}$$

3.3 | Ambiguity Function Analysis

The radar ambiguity function for the angle-dependent waveform is:

$$\chi(\tau, f_d;\theta,\phi) = \int_{-\infty}^{\infty} s(t;\theta,\phi)s^*(t+\tau;\theta,\phi)e^{j2\pi f_d t}dt \tag{8}$$

where $s(t;\theta,\phi)$ is the transmitted waveform at angles (θ,ϕ):

$$s(t;\theta,\phi) = \text{rect}\left(\frac{t}{T(\theta,\phi)}\right)e^{j\pi\frac{B(\theta,\phi)}{T(\theta,\phi)}t^2} \tag{9}$$

The matched filter output becomes:

$$|y(t)| = \left|\int_{-\infty}^{\infty} r(\tau)s^*(\tau - t;\theta,\phi)d\tau\right| \tag{10}$$

This achieves optimal processing gain for targets at the specific angles.

4 | Cramér–Rao Bound Analysis

Consider a target at position $\mathbf{p} = [r,\theta,\phi]^T$. The received signal after demodulation can be modelled as:

$$r(t) = \alpha s(t-\tau;\mathbf{p}) + n(t) \tag{11}$$

where α is the complex amplitude, $\tau = \frac{2r}{c}$ is the time delay, and $n(t)$ is complex Gaussian noise with PSD N_0.

4.1 | Fisher Information Matrix

For parameter estimation, the Fisher information matrix (FIM) elements for parameters λ_i and λ_j are given by:

$$[I(\lambda)]_{i,j} = \frac{2}{N_0}\Re\left\{\int_{-\infty}^{\infty}\frac{\partial s^*(t;\lambda)}{\partial\lambda_i}\frac{\partial s(t;\lambda)}{\partial\lambda_j}dt\right\} \tag{12}$$

4.2 | CRB for Classical Waveform

For the classical approach with fixed parameters B_0 and T_0, the transmitted waveform is:

$$s_{\text{classical}}(t) = \text{rect}\left(\frac{t}{T_0}\right)e^{j\pi\frac{B_0}{T_0}t^2} \tag{13}$$

Following the CRB formalism of [14], for a linear frequency modulation (LFM) waveform with rectangular envelope, the mean-square frequency of the waveform $\bar{\omega}^2 = (2\pi)^2\beta^2T_0^3/12$ yields the CRB for range (time-delay) estimation as:

$$\text{CRB}_r^{\text{classical}} = \frac{c^2}{8\pi^2\beta^2T_0\cdot\text{SNR}} \tag{14}$$

where $\beta = B_0/T_0$ is the chirp rate [15]. For angular parameters, the CRBs depend on the antenna pattern derivatives. For a directive antenna with BW Θ, we have approximately:

$$\text{CRB}_\theta^{\text{classical}} \approx \frac{\Theta^2}{\text{SNR}}, \quad \text{CRB}_\phi^{\text{classical}} \approx \frac{\Theta^2}{\text{SNR}\cdot\sin^2\theta} \tag{15}$$

4.3 | CRB for Angle-Dependent Waveform

Applying the same CRB derivation [14] to the angle-dependent LFM waveform with parameters $B(\theta,\phi)$ and $T(\theta,\phi)$, the range estimation bound becomes:

$$\text{CRB}_r^{\text{adaptive}} = \frac{c^2}{8\pi^2\beta(\theta,\phi)^2T(\theta,\phi)\cdot\text{SNR}(\theta,\phi)} \tag{16}$$

where $\beta(\theta,\phi) = \frac{B(\theta,\phi)}{T(\theta,\phi)}$ is the angle-dependent chirp rate. Substituting the modulation functions from Equation (2) directly into the Fisher information matrix entry $I_{rr} = (8\pi^2/c^2)\beta^2(\theta,\phi)T(\theta,\phi)\text{SNR}(\theta,\phi)$ yields the CRB ratio derived in Equations (17) and (18) below. Algorithm 1 summarizes the angle-dependent waveform optimization.

ALGORITHM 1 | Angle-dependent waveform optimization.

Input: Default parameters B_0, T_0; initial target detections from surveillance scan
Output: Optimized waveform parameters $B(\hat{\theta},\hat{\phi})$, $T(\hat{\theta},\hat{\phi})$ per target
Initialize radar with default waveform parameters (B_0,T_0);Perform initial scan using default parameters;
for *each detected target* **do**
  Estimate target angles $(\hat{\theta},\hat{\phi})$ from initial returns;"Compute $B(\hat{\theta},\hat{\phi}) = \frac{B_0}{\cos\hat{\theta}}$ and $T(\hat{\theta},\hat{\phi}) = T_0(1+\sin^2\hat{\theta})$;
  Generate and transmit optimized LFM waveform;
  Process received signal using matched filtering;
  Update target angle estimates $(\hat{\theta},\hat{\phi})$;
  Repeat these steps for tracking;"

4.4 | CRB Comparison

For range estimation, the ratio of CRBs is:

$$\frac{\text{CRB}_r^{\text{adaptive}}}{\text{CRB}_r^{\text{classical}}} = \frac{\beta_0^2T_0\cdot\text{SNR}_0}{\beta(\theta,\phi)^2T(\theta,\phi)\cdot\text{SNR}(\theta,\phi)} \tag{17}$$

Substituting our modulation functions:

$$\frac{\text{CRB}_r^{\text{adaptive}}}{\text{CRB}_r^{\text{classical}}} = \cos^2\theta \tag{18}$$

For elevation angles $\theta \neq 0$, we have $\text{CRB}_r^{\text{adaptive}} < \text{CRB}_r^{\text{classical}}$. This proves that the angle-dependent waveform provides better range estimation performance for off-boresight targets.

4.5 | BW Modulation Analysis

Figure 1 shows angle-dependent BW modulation over elevation and azimuth. BW scales with elevation as $1/\cos\theta$, independent of azimuth. At high elevations ($\approx$80°), it increases nearly tenfold, significantly improving range resolution along the radar LoS.

5 | Simulation Analysis

Simulations used default bandwidth ($B_0 = 10$ MHz) and pulse duration ($T_0 = 1$ μs) across 0°–80° elevation for 3D analysis.

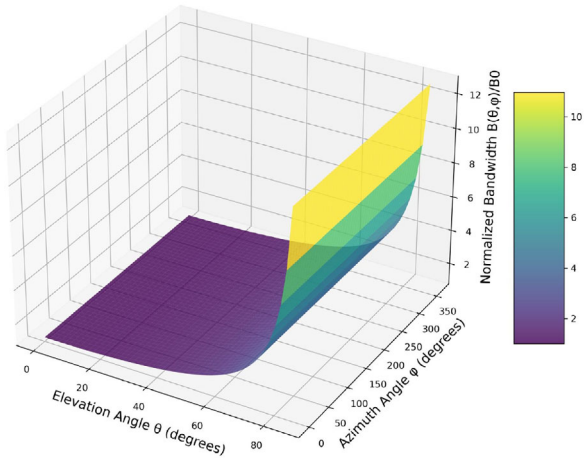

FIGURE 1 | Angle-dependent BW modulation illustrating normalized bandwidth $B(\theta,\phi)/B_0$ versus elevation/azimuth. Bandwidth increases with elevation via $1/\cos(\theta)$ to compensate for geometric projection effects at high angles.

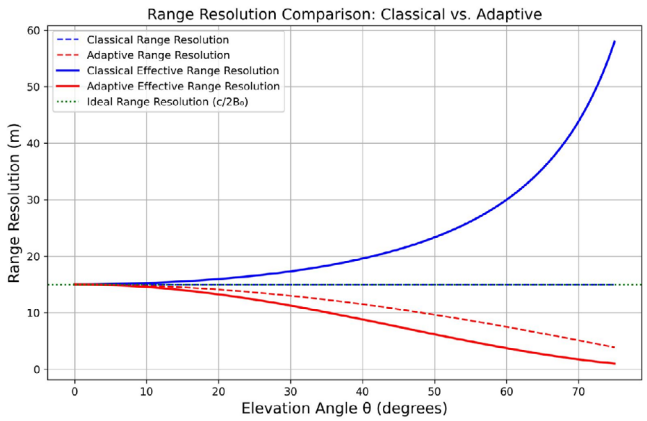

FIGURE 2 | Range resolution comparison: classical (blue) degrades with elevation, adaptive (red) maintains near-ideal performance (green) versus angles.

Figure 2 compares range resolution: classical resolution degrades with elevation, whereas the adaptive approach remains nearly constant. At 60°, the classical method performs ∼4× worse than boresight, while the adaptive approach preserves optimal resolution. Figure 3 presents the CRB ratio for range estimation, matching the theoretical $\cos^2\theta$ trend and confirming gains: equal at 0°, and improvements of 25% at 30°, 50% at 45° and 75% at 60°.

5.1 | 3D Target Scenario Analysis

To assess realistic performance, we simulated multiple targets at random 3D positions. Figure 4 shows results with targets coloured by CRB improvement. Improvements grow with elevation, reaching up to 95% better parameter estimation at high angles. We evaluated five scenarios with distinct elevation profiles: boresight (0°–10°), low (15°–25°), mid (30°–40°), high (50°–60°) and mixed (5°, 25°, 45°, and 65°). Table 1 summarizes results: the high-angle case yields the largest gains with ∼67% CRB, 82% range resolution and 2.2 dB SNR improvement. Even in the mixed

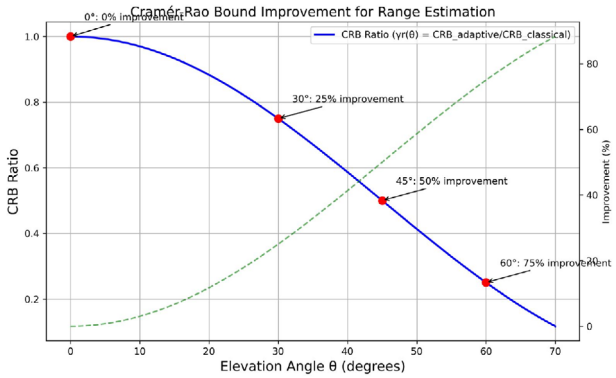

FIGURE 3 | CRB improvement for range estimation, with $\gamma_r(\theta)$ (blue) as the CRB ratio and improvement percentage (green), versus angles.

scenario, notable benefits remain of 38% CRB and 61% range resolution improvement.

5.2 | Impact on Doppler Velocity Estimation

The angle-dependent pulse duration $T(\theta,\phi)$ directly affects Doppler frequency resolution. The minimum resolvable Doppler frequency shift is:

$$\Delta f_d(\theta) = \frac{1}{T(\theta,\phi)} = \frac{1}{T_0(1+\sin^2\theta)}, \tag{19}$$

which is narrower (finer resolution) than the fixed-parameter baseline $\Delta f_{d,0} = 1/T_0$ by a factor of $(1+\sin^2\theta)$. The corresponding minimum resolvable radial velocity step is:

$$\Delta v_r(\theta) = \frac{\lambda}{2T(\theta,\phi)} = \frac{\lambda}{2T_0(1+\sin^2\theta)}. \tag{20}$$

At $\theta = 60°$, for example, $T(\theta,\phi) = 1.75\,T_0$, yielding a 43% improvement in Doppler resolution. This finer discrimination is beneficial for target classification, enabling better separation of targets with closely spaced radial velocities at high elevation angles. The unambiguous Doppler range is unaffected since the PRF is held constant, so the gain is purely in Doppler frequency resolution. This improved Doppler discrimination complements the enhanced range resolution provided by the bandwidth adaptation $f_B(\theta,\phi)$, together supporting more reliable target detection and classification across the full angular coverage.

5.3 | Impact on Scan Time and Update Rate

The angle-dependent pulse extension increases the per-dwell time at each beam position, directly affecting the total scan time and measurement update rate. For a beam at elevation θ_k, the dwell time becomes:

$$\begin{aligned} t_{\text{dwell}}(\theta_k) &= T(\theta_k,\phi)\,(1+\text{PRI overhead}) \\ &\approx T_0(1+\sin^2\theta_k)\cdot\frac{1}{1-\text{DC}} \end{aligned} \tag{21}$$

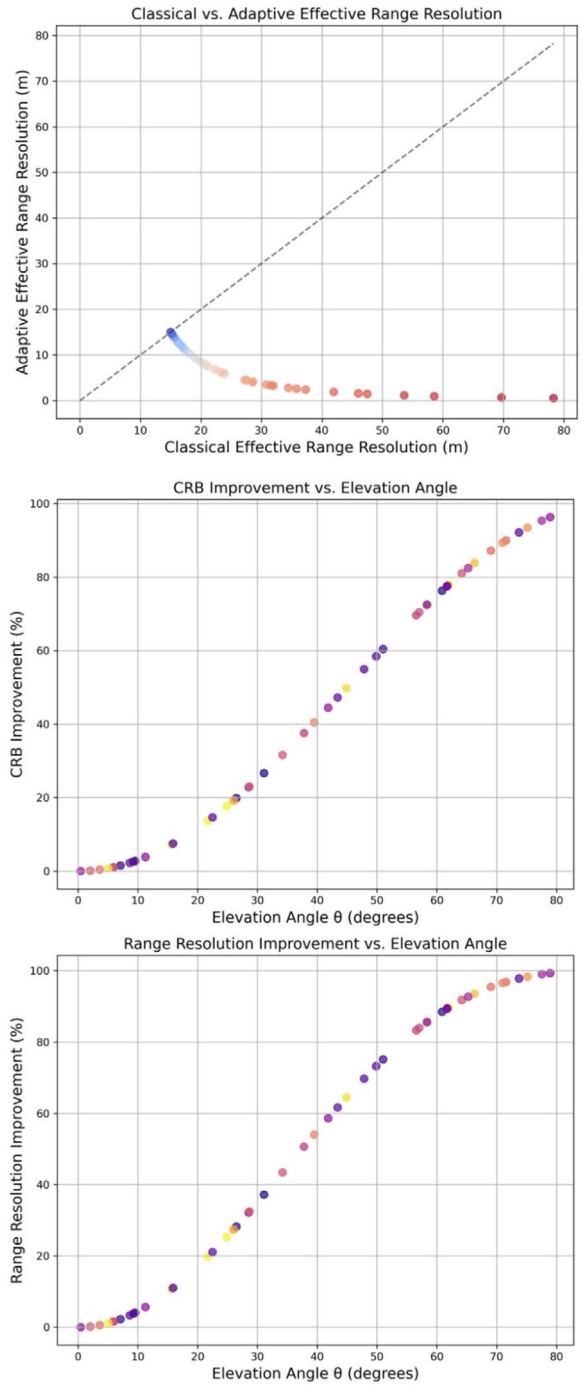

FIGURE 4 | Classical versus adaptive range resolution (1st), CRB improvement versus elevation (2nd) and resolution improvement versus elevation (3rd).

where $\mathrm{DC} = T(\theta_k, \phi) \cdot \mathrm{PRF}$ is the duty cycle. Summing over all N_b beam positions confirms that the total scan time exceeds the fixed-parameter baseline:

$$T_{\text{scan}} = \sum_{k=1}^{N_b} t_{\text{dwell}}(\theta_k) > N_b\, t_{\text{dwell},0}. \tag{22}$$

For a typical surveillance configuration with $N_b = 48$ beams spanning 0°-80° uniformly, the mean value of f_T across all beams is approximately 1.33, increasing total scan time by 33% relative to the baseline. This reduces the measurement update rate from ≈1.0 Hz to ≈0.75 Hz. For slow-moving or high-elevation targets (e.g., hovering UAVs, ballistic targets near apogee), this trade-off is acceptable given the substantial estimation accuracy gains. For fast-manoeuvring targets requiring frequent updates, a hybrid strategy, applying pulse extension only for beams at $\theta > 30°$, limits the scan time penalty to ≈15% while retaining more than 85% of the CRB improvement for high-elevation targets. System designers should select the adaptation strategy based on the predominant target kinematics in the intended operational scenario.

TABLE 1 | Improvement metrics across operational scenarios.

Scenario	CRB improv. (%)	Range res. improv. (%)	SNR improv. (dB)
Boresight	1.3	1.9	0.1
Low-angle	12.1	17.7	0.5
Mid-angle	33.1	45.6	1.2
High-angle	66.9	81.5	2.2
Mixed	37.7	61.0	1.3

6 | Conclusion

This paper analyses angle-dependent waveform design for 3D radar, demonstrating that parameter adaptation yields significant gains. Bandwidth modulation compensates for geometric projection, maintaining uniform range resolution, while pulse-duration modulation enhances SNR. Results show range estimation CRB follows a $\cos^2\theta$ trend, improving up to 75% at 60° elevation. Multi-target tests confirm these benefits. Utilizing digital generators and advanced processing, this method integrates into phased arrays without hardware changes. Future research will address dynamic targets and joint adaptation. Additionally, interference-robust design, balancing wide-angle coverage with interference mitigation, remains a critical open challenge.

Author Contributions

Amgad A. Salama contributed to the conceptualisation of the study and led the methodology, formal analysis and investigation. He also prepared the manuscript's original draft. Ahmed G. Abdellatif contributed to the methodology and investigation, supported the software implementation and validation, and participated in drafting the manuscript. Syed T. Shah contributed to the study's conceptualisation and provided overall supervision and project administration. He also reviewed and edited the manuscript. Ahmad Al Mogren contributed to the formal analysis, provided resources, and reviewed and edited the manuscript. Mahmoud A. Shawky provided methodology, validation, visualization, formal analysis, and secured funding for the project, and also reviewed and edited the manuscript.

Acknowledgements

This work was supported by King Saud University, Riyadh, Saudi Arabia, through Ongoing Research Funding program - Research Chairs, (ORF-RC-2026-24-01).

Conflicts of Interest

The authors declare no conflicts of interest.

Data Availability Statement

Data sharing is not applicable to this article as no datasets were generated or analysed during the current study.

References

1. A. Hassanien, M. G. Amin, Y. D. Zhang, and F. Ahmad, "Dual-Function Radar-Communications: Information Embedding Using Sidelobe Control and Waveform Diversity," *IEEE Transactions on Signal Processing* 64, no. 8 (2015): 2168–2181.

2. D. Cohen, K. V. Mishra, and Y. C. Eldar, "Spectrum Sharing Radar: Coexistence via Xampling," *IEEE Transactions on Aerospace and Electronic Systems* 54, no. 3 (2017): 1279–1296.

3. F. Roos, J. Bechter, C. Knill, B. Schweizer, and C. Waldschmidt, "Radar Sensors for Autonomous Driving: Modulation Schemes and Interference Mitigation," *IEEE Microwave Magazine* 20, no. 9 (2019): 58–72.

4. J. Liu, H. Li, and B. Himed, "Joint Optimization of Transmit and Receive Beamforming in Active Arrays," *IEEE Signal Processing Letters* 21, no. 1 (2013): 39–42.

5. A. Aubry, A. De Maio, M. Piezzo, M. M. Naghsh, M. Soltanalian, and P. Stoica, "Cognitive Radar Waveform Design for Spectral Coexistence in Signal-Dependent Interference," in *2014 IEEE Radar Conference* (IEEE, 0474–0478).

6. A. A. Ahmad, S. A. Ahmad, and A. L. Muhammad, "Recent Developments in the Use of Time-Frequency Analysis for Radar-Based Applications," AFRICON 2015 (IEEE, 2015), 1–5.

7. M. A. Richards, J. A. Scheer, and W. A. Holm, *Principles of Modern Radar: Basic Principles* (IET, 2010).

8. W. Chen, W. Xie, and Y. Wang, "Range-Dependent Ambiguous Clutter Suppression for Airborne SSF-STAP Radar," *IEEE Transactions on Aerospace and Electronic Systems* 58, no. 2 (2021): 855–867.

9. A. Merline and S. Thiruvengadam, "Multiple-Input Multiple-Output Radar Waveform Design Methodologies," *Defence Science Journal* 63, no. 4 (2013): 393.

10. L. Wang, W. Zhu, Y. Zhang, Q. Liao, and J. Tang, "Multi-Target Detection and Adaptive Waveform Design for Cognitive MIMO radar," *IEEE Sensors Journal* 18, no. 24 (2018): 9962–9970.

11. P. Zhu, J. Liang, Z. Luo, and X. Shen, "Cognitive Radar Target Tracking Using Intelligent Waveforms Based on Reinforcement Learning," *IEEE Transactions on Geoscience and Remote Sensing* 61 (2023): 1–15.

12. S. Z. Gurbuz, H. D. Griffiths, A. Charlish, M. Rangaswamy, M. S. Greco, and K. Bell, "An Overview of Cognitive Radar: Past, Present, and Future," *IEEE Aerospace and Electronic Systems Magazine* 34, no. 12 (2020): 6–18.

13. M. I. Skolnik, et al., *Introduction to Radar Systems*, Vol 3 (McGraw-Hill, 1980).

14. M. K. Steven, et al., "Fundamentals of Statistical Signal Processing," *Prentice Hall, Profressional, Technical, Reference* 10, no. 151045 (1993): 148.

15. N. Levanon and E. Mozeson, *Radar Signals* (Wiley, 2004).